



ELSEVIER

Contents lists available at SciVerse ScienceDirect

Deep-Sea Research I

journal homepage: www.elsevier.com/locate/dsri

Water mass pathways and transports over the South Scotia Ridge west of 50°W

Margarita Palmer^{a,*}, Damià Gomis^a, Maria del Mar Flexas^a, Gabriel Jordà^a, Loïc Jullien^b, Takamasa Tsubouchi^b, Alberto C. Naveira Garabato^b

^a Mediterranean Institute for Advanced Studies (UIB-CSIC), Esporles 07190, Spain

^b National Oceanography Centre, Southampton SO14 3ZH, United Kingdom

ARTICLE INFO

Article history:

Received 25 March 2011

Received in revised form

20 October 2011

Accepted 24 October 2011

Available online 3 November 2011

Keywords:

South Scotia Ridge

Warm Deep Water

Weddell Sea Deep Water

Water mass modification

Inverse model

SASSI

ABSTRACT

During the ESASSI cruise carried out in January 2008, a sector of the South Scotia Ridge west of the South Orkney Islands was surveyed with a spatial resolution of 1–2 nm (1 nm ≡ 1852 m) over the continental slopes and of about 5 nm elsewhere. We use the ESASSI-08 data set to quantify the export and regional pathways of waters from the Weddell Sea into the Scotia Sea west of 50°W, where the intermediate and deep waters are characterized by being colder and fresher than those crossing the deeper gaps east of the South Orkney Islands. An inverse model initialized with ship-borne ADCP velocities is applied to temperature and salinity profiles to obtain a better estimation of the flow pattern. The model domain encloses the region between Elephant Island and 50°W, and is delimited north and south by the flanks of the ridge. The value obtained for the full-depth net transport into the Scotia Sea is 7 ± 5 Sv (1 Sv ≡ 10^6 m³ s⁻¹), with heat- ('enthalpy' for a non-zero volume transport) and salt-anomaly fluxes of 14 ± 5 TW and $(0.8 \pm 0.4) \times 10^6$ kg s⁻¹ relative to mean property values of -0.29 °C and 34.56, respectively. The clockwise circulation within the Hesperides Trough enables the along isopycnal exchange of properties between the involved water masses and some diapycnal mixing between the deepest layers. Approximately one-third of the volume transport measured along the northern wall of the trough recirculates inside the trough. The other two-thirds are suggested to outflow into the Scotia Sea, mainly through the deepest gap west of the South Orkney Plateau.

© 2011 Elsevier Ltd. All rights reserved.

1. Introduction

In the Scotia Sea the waters of the Antarctic Circumpolar Current (ACC) are fresher and colder than those carried from the Drake Passage, which indicates the key role of that region in the ventilation of the Southern Ocean. This results in abrupt horizontal gradients of most water properties below the salinity maxima of the Circumpolar Deep Water (CDW), the main constituent of the ACC (Locarnini et al., 1993). Lateral and vertical mixing are thought to be the basic processes for the ventilation of the CDW. Lateral ventilation along isopycnals was shown by Whitworth et al. (1994). Naveira Garabato et al. (2003) obtained intense diapycnal mixing rates with an almost zero net transport between layers of CDW and Weddell Sea Deep Water (WSDW). The latter is the main constituent of the Weddell Sea bottom waters outflowing into the Scotia Sea through the gaps of the South Scotia Ridge (SSR, Naveira Garabato et al., 2002a).

In the Scotia Sea, CDW is characterized by a relative temperature maximum (Upper CDW, or UCDW) and a salinity maximum (Lower CDW, or LCDW) at about 400–500 m depth. Beyond the southern boundary of the ACC (defined by Orsi et al., 1995), LCDW is the only constituent of CDW and it is delimited by the 27.95 and 28.27 kg m⁻³ neutral density isopycnals (Whitworth et al., 1998). A branch of this water turns southwards through the Southwest Indian Ridge discontinuity (Orsi et al., 1993), enters the cyclonic circulation of the Weddell Sea (Weddell Gyre) and reaches again the SSR region, now on its southern flank. Along the way, the core temperature and salinity maxima are eroded and the density of the upper limit increases to 28.10 kg m⁻³. This modified water mass is referred to as Warm Deep Water (WDW) and occupies most of the open-sea water column in the Weddell Sea. The region where waters from the Weddell Sea and Scotia Sea merge is referred to as the Weddell–Scotia Confluence. Of particular importance is the western sector of the SSR, where the Weddell Gyre's waters ($\theta_{\max} > 0$ °C; Deacon and Foster, 1977) mix with the colder ($\theta_{\max} < 0$ °C; Deacon and Foster, 1977), fresher, and oxygen-rich waters from the continental shelves of the tip of the Antarctic Peninsula (Patterson and Sievers, 1980) before spreading into the Scotia Sea.

* Corresponding author. Tel.: +34 971611408; fax: +34 971 61 17 61.
E-mail address: marga.palmer@uib.es (M. Palmer).

Above and below the CDW and WDW lie the Antarctic Surface Water (AASW) and the Antarctic Bottom Water (AABW), respectively. AASW include all the different surface water masses located to the south of the Polar Front of the ACC. The interaction with ice and with the atmosphere is the cause of the wide spatial and temporal variability of AASW. Thus, Shelf Water (SW) results from ocean–ice interactions (Whitworth et al., 1998), while Winter Water (WW) is the subsurface remnant of the cold, surface winter water after the summer warming of the first meters of the water column (Mosby, 1934). AABW originates in the Weddell Sea from the intrusion and mixing of SW with WDW. Defined by a neutral density $> 28.27 \text{ kg m}^{-3}$, it is separated in Weddell Sea Deep Water (WSDW, $\theta > -0.7^\circ\text{C}$) and Weddell Sea Bottom Water (WSBW, $\theta < -0.7^\circ\text{C}$) (Reid et al., 1977). The characteristics of AABW are conditioned by the local properties of SW (Orsi et al., 1999), but the bottom waters of the Weddell Sea are particularly important for the ventilation of the Southern Ocean because they are historically fresher and colder than the bottom waters of the Ross Sea, the second region in bottom water formation.

The hydrodynamic structure of the northern boundary of the Weddell Gyre is crucial to understand the outflow of cold ventilated waters from the Weddell Sea into the Scotia Sea. Along the northeastern slopes of the Antarctic Peninsula there is a continuous mixing of shelf waters with waters from the Weddell Gyre; it is this branch of cooled and freshened Weddell Gyre waters that flows into the Powell Basin (Fig. 1) along its outer rim and then spreads into the Scotia Sea through the gaps located to the west of the South Orkney Plateau (Gordon et al., 2001). A less modified inner branch continues eastwards along the southern rim of the basin, surrounds the South Orkney Plateau and outflows into the Scotia Sea through the gaps located to the east of the South Orkney Islands (Gordon et al., 2001).

Previous studies on the outflow of Weddell Sea waters into the Scotia Sea have mostly focused on bottom waters and on the deeper, eastern gaps of the SSR. The different cruises and

methodologies used to estimate the transports through the Orkney Passage show an overall agreement for the WSDW outflow: results from inverse models are between the $3.48 \pm 1.81 \text{ Sv}$ ($1 \text{ Sv} \equiv 10^6 \text{ m}^3 \text{ s}^{-1}$) given by Franco et al. (2007) and the $5.6 \pm 0.1 \text{ Sv}$ given by Naveira Garabato et al. (2002b), while ocean circulation models give mean annual transports of 4.2 Sv with a seasonal variability of 0.3 Sv (Schodlok et al., 2002). Naveira Garabato et al. (2003) also give some figures for the net flow over the whole SSR: $19 \pm 7 \text{ Sv}$ for the entire water column, of which $6.0 \pm 1.5 \text{ Sv}$ would correspond to bottom waters and $10.5 \pm 5 \text{ Sv}$ to LCDW/WDW.

The outflow through the gaps west of the South Orkney Islands is much more uncertain: the annual mean WSDW transport of 2.2 Sv with a seasonal variability of 0.2 Sv obtained by Schodlok et al. (2002) contrasts with the $0.12 \pm 0.03 \text{ Sv}$ and the $-0.1 \pm 0.3 \text{ Sv}$ given by Franco et al. (2007) and Naveira Garabato et al. (2002b), respectively. Franco et al. (2007) suggested that the differences among the reported values could be due to the different sampling strategies and methodologies of the analysis. These would be particularly critical when the flow is constrained by a complex topography and subjected to a marked temporal variability derived from the presence of meanders and narrow jets, as it is west of 50°W . The western gaps of the SSR are shallower than the eastern gaps, and therefore only the lighter components of bottom waters are allowed to overcross west to the South Orkney Islands. However, the fact that the western path is shorter and carries colder and fresher water than the eastern branch suggests that it can also play a significant role in the ventilation of the Scotia Sea.

The objective of this work is to present an accurate quantification of the transport of volume, heat, and salt through the gaps of the northern and southern flanks of the SSR west of the South Orkney Islands, and more particularly for those located west of 50°W . We also intend to quantify the flow that surrounds the Hesperides Trough, a key topographic feature located in between the northern and southern flanks of the ridge. The study is based on the data collected during the ESASSI-08 cruise, carried out in

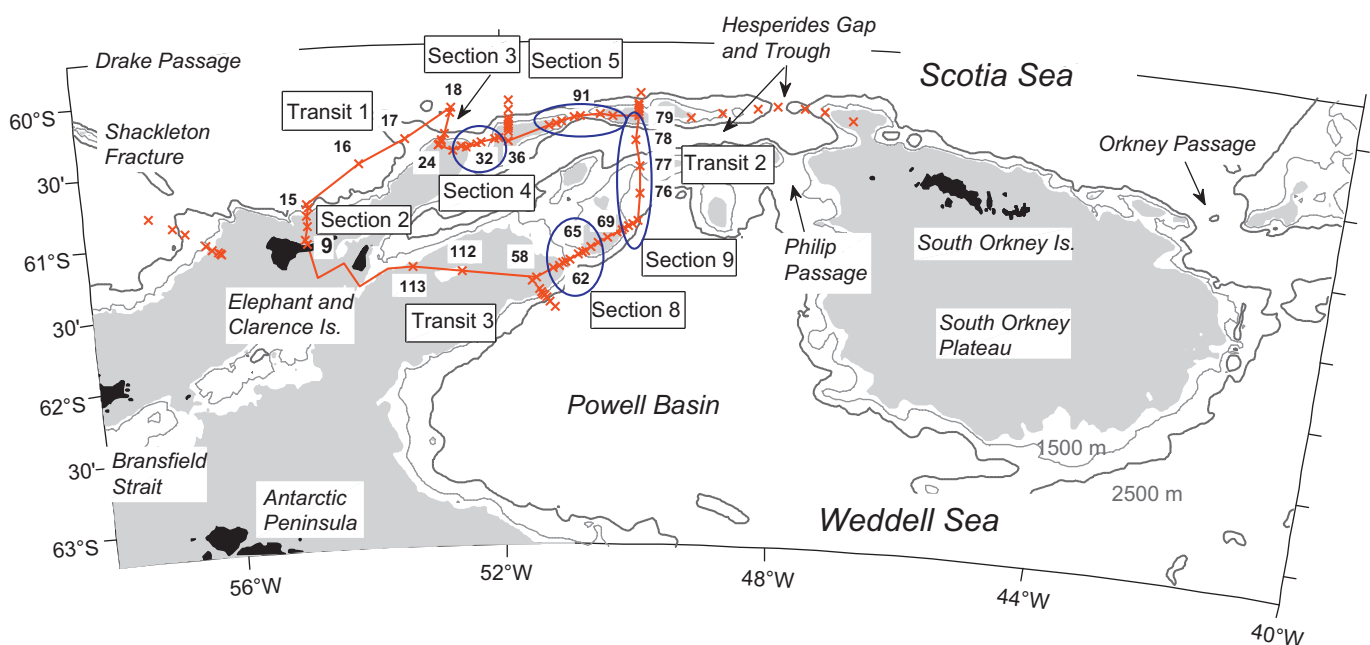


Fig. 1. ESASSI-08 hydrographic stations (red crosses) in the region. The stations constituting the model box are linked; only the most relevant are numbered. The bathymetry is from Smith and Sandwell (1997); the areas shallower than 1000 m are shaded. The topographical gaps crossed by the boundaries of the model domain have been encircled: one of them is in the southern flank of the South Scotia Ridge (section 8) and two in the northern flank (sections 4 and 5). The eastern boundary of the box (transit 2) runs from the southern flank to the northern flank. (For interpretation of the references to color in this figure legend, the reader is referred to the web version of this article.)

January 2008 onboard the R.V. *Hespérides*. Sections across the different gaps that indent the SSR were sampled with a high spatial resolution, which allows an accurate representation of shelf-slope features. Absolute velocities have been first estimated from CTD casts and ship-borne ADCP data and then corrected using an inverse model.

A brief description of the ESASSI-08 data set, the water mass distribution over the western sector of the SSR, and the consequent set up of the inverse model are presented in Section 2. The application of the inverse model and the analysis of its impact on the velocity field are presented in Section 3. The analysis of the results yielding the regional circulation (quantifications of the transports and water mass pathways) is presented in Section 4. Conclusions are outlined in Section 5.

2. Inverse model design

Inverse modeling (Wunsch, 1977) allows correcting the velocity field by applying flow conservation equations to layers in the water column (Table 1) in an enclosed region of the ocean assumed to be in geostrophic balance. For this work, we use DOBOX, implemented by Morgan (1994) and tested against a numerical model by McIntosh and Rintoul (1997).

2.1. Box domain and ESASSI-08 data set

The domain for the inversion covers from 60°S (the northern flank of the SSR) to 61.5°S (the southern flank) and from Elephant Island to 50°W (Fig. 1). The box makes use of six of the hydrographic sections sampled during the ESASSI-08 cruise, with closely spaced stations (1–2 nm over the slope, less than 5 nm elsewhere, 1 nm ≡ 1852 m) covering the main passages of the northern and southern flanks of the SSR. The box also uses three transits extending along greater distances but with fewer stations. Direct current measurements from a ship-borne ADCP were collected along all the sections and transits.

The most important gaps crossed by the box model are the two westernmost gaps of the southern flank (2100 and 2500 m depth, sections 8 and 9, respectively), the Hesperides Trough (4000 m depth, northern part of transit 2), and the two westernmost gaps of the northern flank (1700 and 1300 m depth, sections 4 and 5, respectively). The ESASSI-08 cruise did not cover the stretch between Elephant and Clarence Islands, and from Clarence Island to the beginning of transit 3. The closure of the box at this site is addressed in the next section.

2.2. Closure of the box

The last hydrographic station of the ESASSI-08 cruise (cast 113, see Fig. 1) is located about 80 km to the E-SE of Elephant Island. No ADCP data were recorded between that cast and Elephant

Table 1
Inverse model layers and water masses delimited by the chosen neutral density surfaces.

Layer	Upper interfaces γ^n (kg m ⁻³)	Water mass
1	Surface	AASW
2	27.95	
3	28.0	LCDW/AASW
4	28.06	
5	28.1	LCDW/WDW
6	28.16	
7	28.23	
8	28.27	WSDW
9	28.31	

Island. Some inflow from the Bransfield Strait has been reported to enter the selected domain through that gap (López et al., 1999) and therefore it must be included in the conservation equations before the inversion of the model equations. The estimation of the property transports across that transect will be based on historical data and on previous results obtained by other authors.

A relevant contribution to the knowledge of the missing transect comes from the hydrographic data collected during the ECOANTAR-94 cruise carried out in January 1994. That is, the same month as the ESASSI-08 cruise, though 14 years earlier. During ECOANTAR-94 the whole eastern basin of the Bransfield Strait was covered with a regular distribution of stations spaced 20 km (López et al., 1999). Those hydrographic data and the baroclinic component of the geostrophic velocities computed with respect to the deepest common level enable the tracking of the water masses exiting the Bransfield Strait to the east, since they cover most of the gap of the ESASSI-08 cruise. The barotropic component of the current cannot be estimated from ECOANTAR-94 data, due to the absence of direct current measurements. Instead, absolute velocities were estimated from near surface velocities recorded by drifters and interpolated over the ECOANTAR-94 station pairs. The analysis of the data set of historical and ADELIE-07 drifters provided by Thompson et al. (2009) shows a negligible barotropic component compared with the geostrophic shear.

The ECOANTAR-94 stations cover most of the missing transect, but there is still a small uncovered segment shallower than 500 m close to the southeast coast of Elephant Island. The hypothesis we make is that the westward flow observed at the northern coast of the island (casts 9–10, section 2) is a coastal current surrounding Elephant Island anti-clockwise, so that the volume transport at the southern coast should be equal to the transport observed to the north of the island.

A previous study of the ECOANTAR-94 cruise (López et al., 1999) estimated the geostrophic flow across the missing transect in approximately 0.5 Sv, of which 0.4 Sv would enter the box domain between Elephant and Clarence Islands and 0.1 Sv would enter the box to the southeast of Clarence. That calculation is based on the hypothesis of a common level of no motion at 500 m depth. A re-calculation down to the bottom and the inclusion of the coastal flow around Elephant Island increase the net volume transport up to 1.4 Sv (Table 2). The lack of synopticity between the drifters and ECOANTAR-94 data as well as the inherent temporal variability of the Bransfield currents (Savidge and Amft, 2009) suggest considering transport uncertainties of the same order as the quoted absolute values.

2.3. Water mass distribution

The vertical distribution of temperature (Fig. 2) shows the main water masses along the box. The AASW and AABW are

Table 2
Estimated property transports across the missing transect needed for the closure of the box domain.

Layer	Volume transport (Sv)	$\Delta\theta$ transport (°C Sv)	ΔS transport (Sv)
1	0.527	0.249	-0.099
2	0.121	-0.004	-0.010
3	0.221	-0.036	-0.008
4	0.183	-0.027	-0.002
5	0.236	-0.013	0.005
6	0.129	0.007	0.007
7	0	0	0
8	0	0	0
9	0	0	0
Full depth	1.417	0.176	-0.106

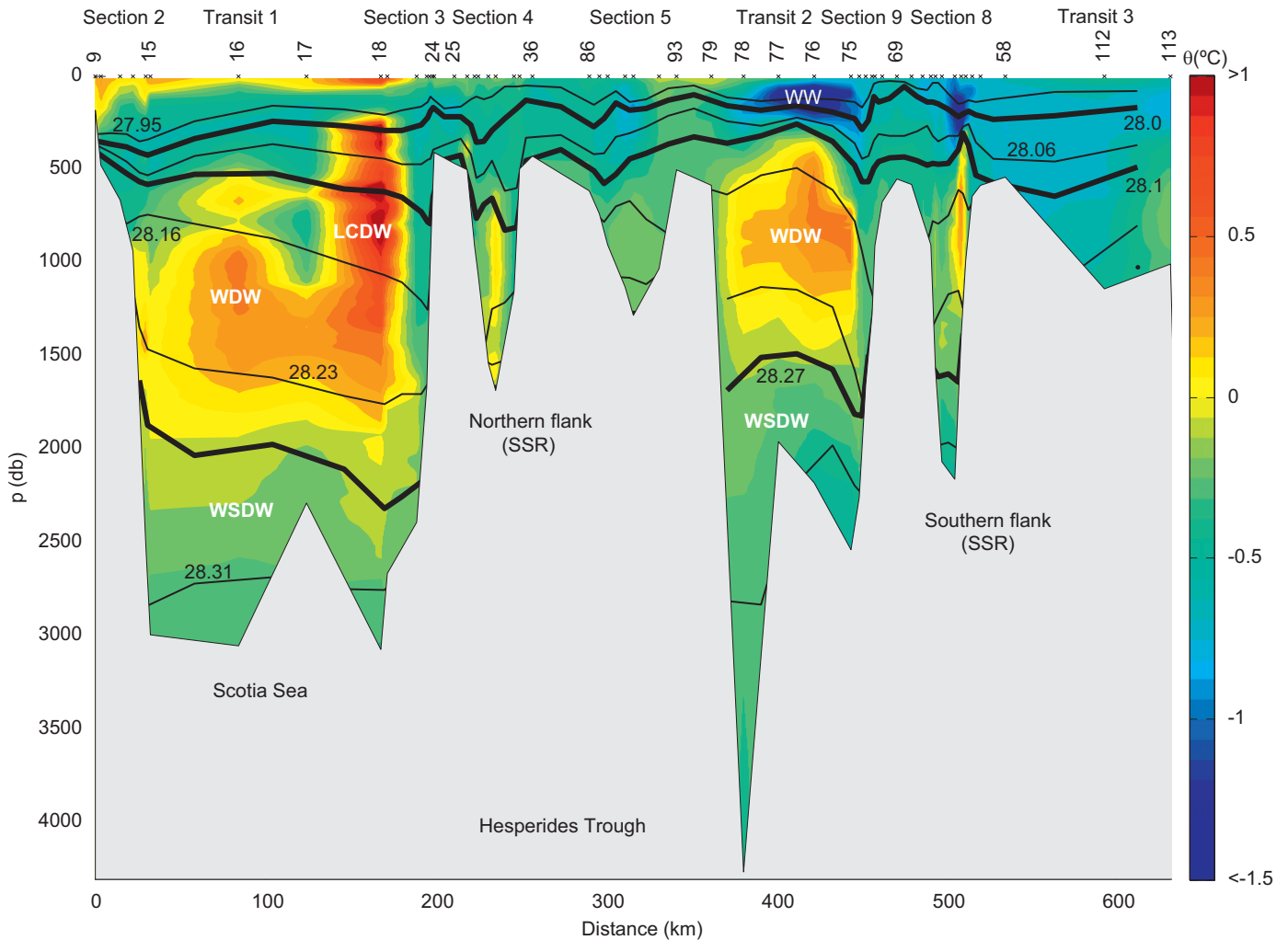


Fig. 2. Vertical distribution of potential temperature along the boundaries of the model. Neutral density interfaces delimiting the model layers (see Table 1) are drawn in black; the thicker lines correspond to 28.00, 28.10, and 28.27 kg m^{-3} .

separated by the relative temperature maximum of the regional Circumpolar Deep Water: the WDW found below the 28.1 kg m^{-3} isopycnal over most of the box domain and the LCDW ($\theta_{\text{max}} > 1^\circ\text{C}$, $S_{\text{max}} > 34.7$) found below the 27.95/28.0 kg m^{-3} isopycnals at the northernmost side of the box (casts 18 and 19, section 3), delimiting the southern boundary of the ACC. The temperatures close to the freezing point ($\theta \approx -1.9^\circ\text{C}$) and high salinities characterizing recently formed SW are not observed in the box.

The surface layer ($\gamma^n < 27.95 \text{ kg m}^{-3}$) occupies the upper 400 m north of Elephant Island (section 2). Its lower interface rises along the rest of the box, almost outcropping over the shelves of both flanks of the ridge (cast 36, between sections 4 and 5 in the northern flank and cast 69, between sections 8 and 9 in the southern flank, Fig. 2). The temperature of the surface layer ranges from -1°C in the southern flank to 0.3°C in the northern flank. The warmest surface water ($\theta \approx 0.7^\circ\text{C}$) overrides the southern boundary of the ACC. The subsurface layers (27.95–28.00–28.06 kg m^{-3}) are located above all the topographic barriers of the region, allowing the free overflowing of AASW. The coldest water mass corresponds to WW, characterized by a temperature minimum located between the 27.95 and 28.0 kg m^{-3} interfaces. Its lowest value ($\theta = -1.6^\circ\text{C}$) is found above the core of the WDW entering the southern flank of the ridge from the Powell Basin (section 8 and transit 2).

Denser waters are more constrained by the bathymetry. WDW (28.1–28.27 kg m^{-3}) is found between 300 and 1500 m at the southern flank (section 8) and in the Hesperides Trough (transit 2), and between 500 and about 2000 m in the Scotia Sea (transit 1). Its temperature–salinity maximum core ($\theta \leq 0.5^\circ\text{C}$, $S < 34.7$) lies just below the 28.16 kg m^{-3} isopycnal. The gaps of the northern flank of the ridge do not show any WDW core: the shallower of the northern gaps (section 5) is filled with an homogeneous, cold water mass ($\theta < 0^\circ\text{C}$), whereas the warmer core of the western gap (section 4) is lighter than the 28.16 kg m^{-3} isopycnal.

The bottom water mass components ($\gamma^n > 28.27 \text{ kg m}^{-3}$) observed in the Scotia Sea and in the Weddell Sea are not directly connected through the northern gaps of the box domain (sections 4 and 5), but they are through the Hesperides Gap (out of the box domain, see Fig. 1). That 3100 m gap is the deepest gap to the west of the South Orkney Islands and connects the Hesperides Trough with the Scotia Sea.

The properties observed at the southern and northern flanks of the ridge and at the southwestern sector of the box (transit 3) are rather different because the complex topography allows the confluence of different open-sea and shelf water masses. In spite of that, the property patterns along 50°W (transit 2, including the Hesperides Trough) seems to be rather stable in time, because similar temperature and salinity distributions were measured in 1975 (Deacon and Foster, 1977).

2.4. Inverse model setup

The set of linear equations used for the inversion accounts for the geostrophic flow across the boundaries of the domain and for internal diapycnal mixing. At the time of the cruise, surface winds (gathered from the NCEP Reanalysis, NOAA/OAR/ESRL PSD, <<http://www.esrl.noaa.gov/psd>>) were predominantly eastward over the region, with values around 6 m s^{-1} . They would result in a net northward flow of about 0.1 Sv for an Ekman layer of 50 m depth. These values are much smaller than the uncertainties derived from the measurement errors and from the temporal variability inherent to the surface of the ocean, then concluding that the Ekman transport is irrelevant for the model inversion.

In the vertical, the conservation is applied to the full-depth and to the layers delimited by the neutral density interfaces (McDougall, 1987) selected for the inversion (Table 1). Each of the four shallower layers covers about 6% of the lateral area, while each of the five deeper layers covers about 15% (Fig. 2). Not only the conservation of volume, but also the conservation of potential temperature and salinity are included in the system, increasing the number of equations (3 properties \times 10 layers) but not reducing the indetermination of the system (78 unknowns from 54 station pairs and 3×8 diapycnal mixing effective velocities) due to the increase in the number of diapycnal mixing unknowns (Wunsch, 1996; Sloyan and Rintoul, 2000). In order to avoid mathematical problems when inverting the matrix equation, the conservation equations for heat and salt are applied to potential temperature and salinity anomalies relative to the local mean values ($\Delta\theta = \theta - \bar{\theta}$, $\Delta S = S - \bar{S}$, Jullion et al., 2010), instead of to absolute values (θ , S) (McDougall, 1991).

3. Velocity field and imbalances before and after the inversion

3.1. First guess of the velocity field and initial imbalances

Previous studies have shown that the assumption of a common level of no motion is not appropriate in the region (Gordon et al., 2001; Naveira Garabato et al., 2002b; Franco et al., 2007). In many cases the barotropic component is as important as the baroclinic one, and inverse models can lead to solutions far from reality if a first guess of the barotropic flow is not considered (Naveira Garabato et al., 2003). The geostrophic shear with respect to the deepest common level and the cross-section, deduced ADCP profiles (ANTPEN, Padman et al., 2002) are shown in the upper panels of Fig. 3. In order to obtain an estimation of the barotropic velocity and then of the first guess of the velocity field (third panel, Fig. 3), we applied Rudnick's method (Rudnick, 1996) to the geostrophic shear and the mean ADCP profile at every station pair. The residuals of the fitting are considered as a measure of the error of the barotropic velocity at every station pair. The obtained errors are bigger than $\pm 0.02 \text{ m s}^{-1}$ everywhere, with extreme values of about $\pm 0.11 \text{ m s}^{-1}$ for some narrow jets over the slope (Fig. 3, lower panel). These errors are mostly due to the noise in the ADCP data and they are not reduced by discarding the Ekman layer (see lower panel in Fig. 3). The smallest errors are obtained at the gaps of the northern flank, at the Hesperides Trough, and at the southern boundary of the ACC. Regarding diapycnal velocities, they are initially set to zero, and their uncertainty is set to $\sim 10^{-5} \text{ m s}^{-1}$, the maximum values observed for mixing processes in the ocean (Orsi et al., 1999).

The transports calculated from the first guess show a clear imbalance (Fig. 4): for single layers the mean residuals are of about 3 Sv, amounting to 25 Sv for the full depth. It is that big imbalance, introduced by the barotropic component, that justifies the use of the inverse method to refine the velocities. The

potential temperature and salinity anomalies show the largest imbalance in the shallower and bottom layers, the potential temperature anomalies show the largest imbalance at subsurface levels (layer 3) and close to the core of WDW (layer 6). Salinity anomalies show the maximum imbalance at the shallower and bottom layers (Fig. 4).

Before the model inversion, the uncertainty of the first guess must be determined and introduced in the equation system. Errors in the volume transport must include the velocity observational errors, but also the temporal variability of each layer. Determining the error of every layer for a box that covers a small region with a complicated topography, where shallow and deep locations are connected by steep slopes, is not straightforward. The errors assigned to every layer and to the full depth should be close to the initial imbalances, that is, about 3 Sv for each layer, with a minimum of 1.2 Sv for the bottom layer and a maximum of 4.5 Sv for the subsurface layers. The volume errors assigned to each layer are presented in Table 3, altogether with the layer mean values of potential temperature and salinity.

The way of introducing the uncertainties of the first guess in the equation system is double weighting the matrix (Wunsch, 1996). We can assign more or less confidence to the conservation in every layer by considering the volume variability and normalizing by twice the standard deviation of the layer mean value of potential temperature and salinity instead of by their means (Table 3), in order to avoid possible unrealistic extremes when the mean value for the layer and for the box are similar (Jullion et al., 2010). The uncertainty of the solution (referred to as 'a posteriori errors') can also be estimated. The method followed here is based on the Gauss–Markov statistical procedure for inverse models developed by Wunsch (1996).

3.2. Final imbalances and absolute velocity field

The system is solved by applying a Singular Value Decomposition technique (Golub and Kahan, 1965). The output from the inversion is the correction to the barotropic component of the velocity, the transports across the walls of the box, and the diapycnal exchanges. The potential temperature and salinity anomalies used to compute the heat- ('enthalpy' for non-zero advection, Ganachaud and Wunsch, 2000) and salt-anomaly transports are estimated with respect to the mean values of potential temperature ($\theta = -0.29 \text{ }^\circ\text{C}$) and salinity ($S = 34.56$) along the box (full depth, Table 3).

Perfect conservation would be reached for the mathematical or maximum rank of the solution (rank=30 in our case), but mathematical instabilities (rank ≥ 27 , for the residual norms in the Levenberg–Marquardt plot of Lawson and Hanson, 1974) and physical unrealistic results are obtained when reaching the complete solution. The effective rank (Wunsch, 1996) is a compromise between velocity changes and conservation forcing, and is usually much smaller than the mathematical rank. The impact on the residuals for the first 12 ranks of the solution is presented in Fig. 4. The first three eigenvalues are essential to reach robust residuals for all properties. On the other hand, the barotropic velocities change more than their a priori errors for rank ≥ 9 , and diapycnal mixing effective velocities become sensitive to the rank for rank ≥ 6 . Therefore we selected the solution corresponding to rank 5; this choice explains 78% of the initial variability, keeps final barotropic velocities inside their initial error margins, and final residuals are not statistically different from zero (they fall within the a posteriori errors). The full-depth residuals are reduced after the inversion from -25 to $-0.6 \pm 1.1 \text{ Sv}$, and from -9 to $-2 \pm 5 \text{ TW}$, whereas the residuals for the salt content remain similar (-0.5×10^6 to $(0.3 \pm 0.5) \times 10^6 \text{ kg s}^{-1}$). The net balance involves the lateral flow, the contribution from the

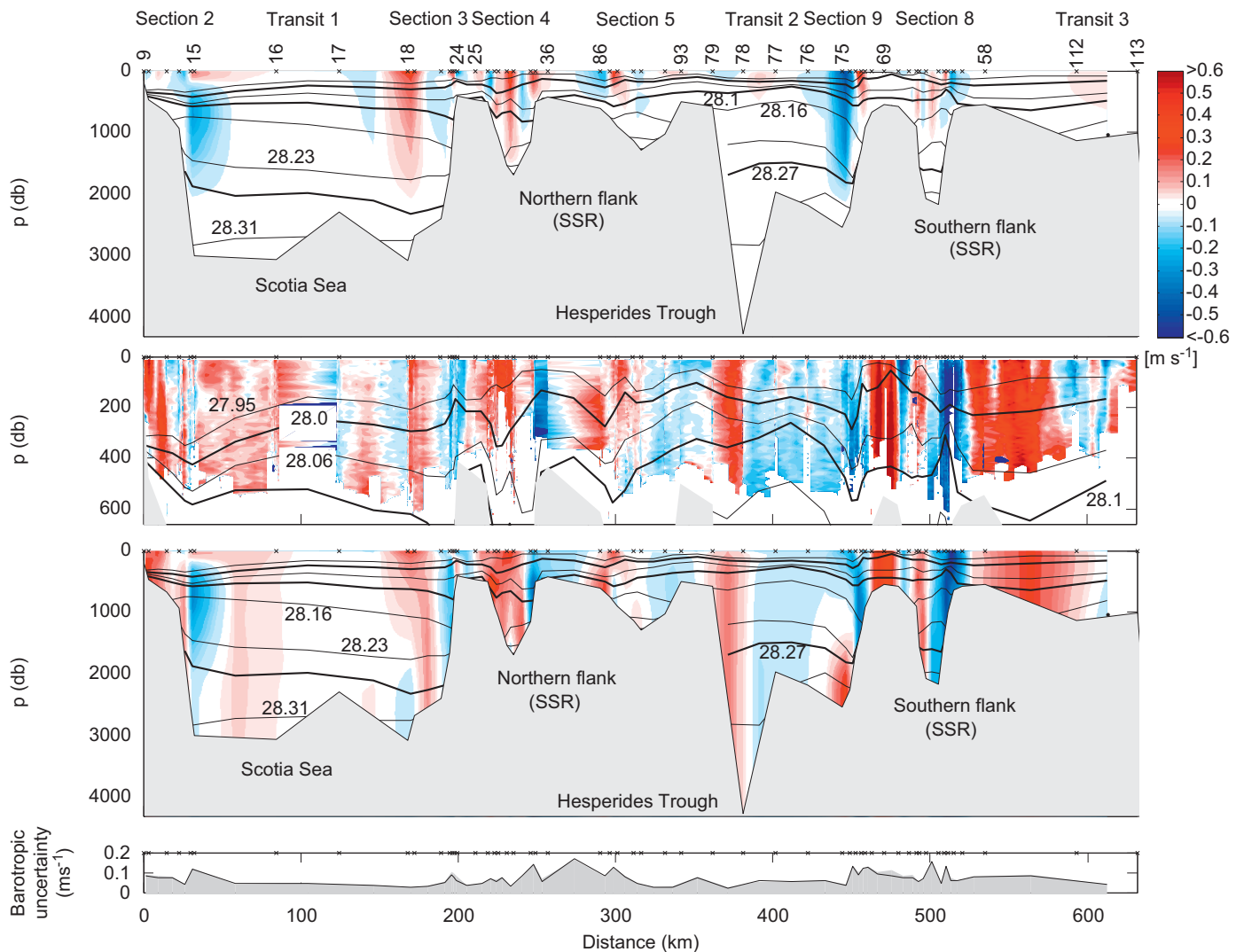


Fig. 3. First guess used to initialize the inverse model: the baroclinic component of the geostrophic field relative to the deepest common level (upper panel), the cross-section de-tided ADCP velocity (second panel) and the total geostrophic velocity field before the inversion (third panel). The black lines are the neutral density model interfaces (the thicker ones correspond to 28.00, 28.10, and 28.27 kg m^{-3}). Positive values denote outward velocities from the box domain. The lower panel shows the uncertainty of the first guess when the ageostrophic terms inferred from the surface winds are removed (thin line) and when they are not (shaded area).

extrapolation to the bottom of the velocity at the deepest common level, and a small contribution from the vertical mixing (volume advection, heat- and salt-anomaly advection-diffusion, Table 4). There is some mixing in the middle layers, with effective velocities of the order of $\sim 10^{-6} \text{ m s}^{-1}$. Note that heat and salt diffusion are obtained at the interface that separates LCDW/WDDW from WSDW. Some salt exchange is also obtained at upper layers.

The sensitivity of the velocity field resulting from the inversion was tested by changing independently some features of the model setup (Fig. 5), such as imposing no fluxes through the missing transect, setting the diapycnal mixing to zero or requiring conservation of only one of the three variables. From all the cases, the barotropic velocity changed more than the a priori error only in a few stations when volume or salinity conservation alone was requested (upper panel, Fig. 5). The differences between the sensitivity tests are much smaller than the velocity correction except in a few locations, so that the overall impact on the velocity field across the walls of the box is small (middle panel, Fig. 5). In any case the initial imbalance was reduced by more than 90%.

Particular attention was paid to the impact of the bottom extrapolation (lower panel, Fig. 5). The bigger bottom triangle areas are found along the transits of the box domain, where the

station separation is larger. Transit 1 is not very relevant for the quantification of the northward exportations, and in Transit 3 the differences between extrapolating or not the velocities fall within the associated uncertainties. Transit 2 deserves more attention, because it crosses the Hesperides Trough and because at the northern station pair (casts 79–78) the area of the bottom triangle is as large as the area of the above levels altogether. After testing different options we decided that the best one was the extrapolation of the velocity obtained at the deepest common level down to the bottom. The reason is that the barotropic component is higher than the baroclinic component in that station pair: the shear is important in the first 200 m, where it ranges from 0.10 to 0.16 m s^{-1} , but below that level the shear is negligible as derived from our data (down to 600 m) and supported by other datasets such as the DOVETAIL (1997) 48°W section, which shows a rather constant LADCP values down to the bottom.

The correction of the barotropic field by the inverse model represents a mean shift of -0.03 m s^{-1} with respect to the first guess (top panel of Fig. 6) and compensates most of the previous imbalance. The maximum velocity correction are the -0.07 m s^{-1} obtained over the shelf that separates the two westernmost gaps of the northern flank (sections 4 and 5) and

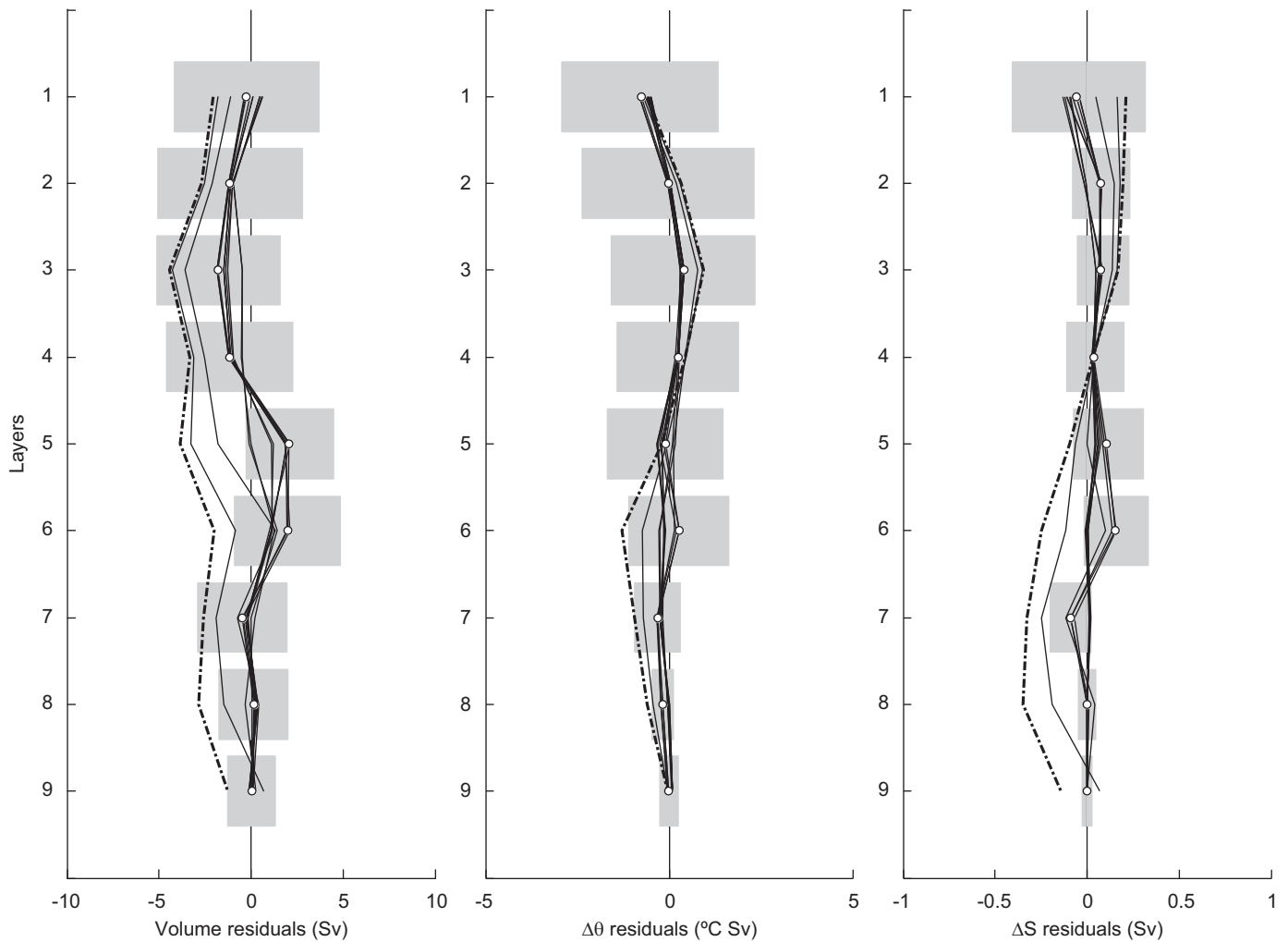


Fig. 4. Residuals before and after the inversion. The dash-dot line represents the initial residuals, thin lines denote the residuals for ranks 1–12, with the selected rank (5) marked with white circles. The a posteriori errors for rank=5 are shown as gray areas.

Table 3

A priori errors for the layers of the conservation system.

Layer	Error (Sv)	Mean \pm std dev θ ($^{\circ}$ C)	Mean \pm std dev S
1	4.0	-0.464 ± 0.267	34.407 ± 0.045
2	4.0	-0.579 ± 0.293	34.466 ± 0.019
3	3.5	-0.521 ± 0.282	34.511 ± 0.020
4	3.5	-0.392 ± 0.237	34.548 ± 0.022
5	3.5	-0.229 ± 0.230	34.586 ± 0.027
6	3.5	-0.018 ± 0.200	34.634 ± 0.025
7	2.5	-0.058 ± 0.124	34.653 ± 0.022
8	2	-0.195 ± 0.072	34.656 ± 0.012
9	1.5	-0.333 ± 0.084	34.655 ± 0.009
Full depth	5	-0.292 ± 0.158	34.564 ± 0.050

the -0.06 m s^{-1} correction to the inflow through section 8. The barotropic velocities and the absolute velocity field for the selected rank of the solution are shown in the middle and lower panels of Fig. 6.

The barotropic velocities have a standard deviation of about $\pm 0.20 \text{ m s}^{-1}$ and there is no correlation ($\rho^2=0.02$) between the intensity of the geostrophic shears and the barotropic velocities. Nevertheless, barotropic velocities up to $\pm 0.30 \text{ m s}^{-1}$ are obtained only where geostrophic shears are smaller than $\pm 0.10 \text{ m s}^{-1}$. Muench and Hellmer (2002) noted that in the northwestern Weddell

Sea the weak stratification entails stronger barotropy. Conversely, where geostrophic velocities are larger than $\pm 0.10 \text{ m s}^{-1}$, the barotropic component is smaller. Thompson and Heywood (2008) observed a similar behavior related to the steepness of the bottom slope for a cross-slope section at the tip of the Antarctic Peninsula. At some of these locations the barotropic velocity has opposite sign to the baroclinic component respect to the deepest common level, yielding bottom undercurrents.

Narrow but strong slope currents are observed flowing to the north/south over the western/eastern flanks of the gaps (that is, leaving shallow areas to the left of the flow). The same holds for the Hesperides Trough, which shows a clear clockwise circulation: outward from the box (to the east) through casts 79–78 and inward (to the west) through casts 77–78 (lower panel of Fig. 6, transit 2).

Regarding the hypothesis of synopticity it is worth noting that ESASSI-08 was a comparatively fast cruise compared with the time that it takes to perform large scale cruises used afterwards to run an inverse model. All stations used in the model were sampled in a 10 day period with the exception of stations 112 and 113 (transit 3, see Fig. 1), which were sampled five days later. The non-synopticity respect to the ECOANTAR-94 casts is not relevant in this case because the sensitivity tests indicate that the results along the box are not sensitive to the flow across that transect.

Table 4
Diapycnal mixing transports for the selected (rank=5) solution.

Layer	Diapycnal volume transport ($10^6 \text{ m}^3 \text{ s}^{-1}$)	Diapycnal $\Delta\theta$ transport (10^{12} W)	Diapycnal ΔS transport (10^6 kg s^{-1})
1	0.00 ± 0.12	0.00 ± 0.10	0.002 ± 0.014
2	-0.01 ± 0.17	0.00 ± 0.15	-0.002 ± 0.015
3	0.01 ± 0.17	0.00 ± 0.13	0.000 ± 0.008
4	-0.02 ± 0.16	0.00 ± 0.07	0.000 ± 0.003
5	0.04 ± 0.15	0.00 ± 0.07	0.001 ± 0.006
6	-0.02 ± 0.12	0.00 ± 0.12	0.002 ± 0.009
7	0.00 ± 0.08	-0.03 ± 0.11	-0.005 ± 0.009
8	0.00 ± 0.06	0.02 ± 0.05	0.007 ± 0.007
9	0.00 ± 0.04	0.00 ± 0.01	-0.005 ± 0.004

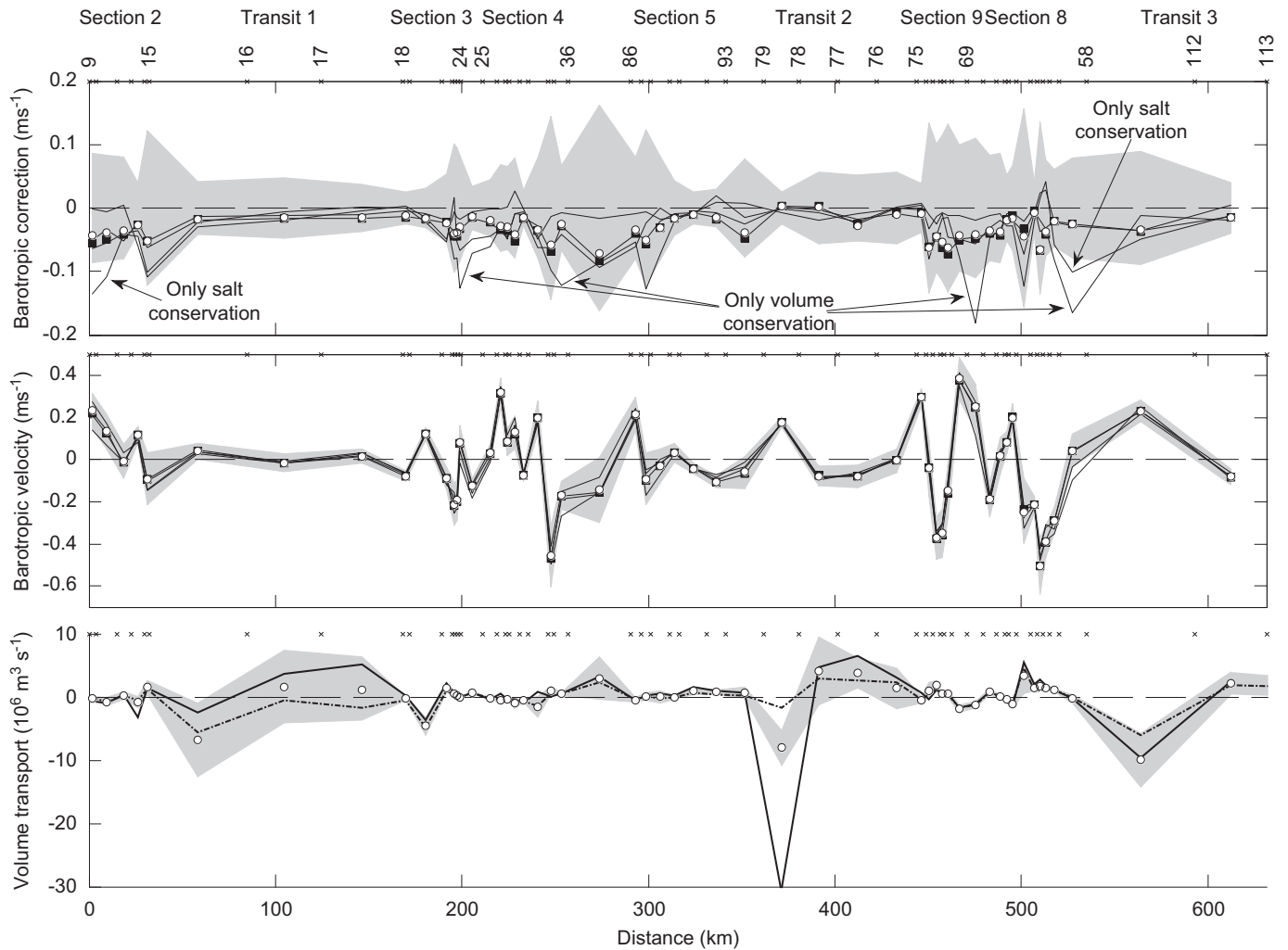


Fig. 5. Correction to the barotropic component, with the initial uncertainty in gray (white circles, upper panel) and barotropic velocities obtained after the inversion with the a posteriori error at rank=5 in gray (white circles, lower panel). When no fluxes are assumed through the missing transect (southwest corner of the box) the obtained correction is denoted by black squares. The results of other sensitivity tests (no diapycnal mixing, only volume conservation, only potential temperature anomaly conservation, and only salinity anomaly conservation) are indicated by thin lines. The lower panel shows the full-depth volume transport obtained when applying the bottom triangle velocity extrapolation (white circles) within the a posteriori error in gray. The dash-dot line corresponds to the transport obtained with no extrapolation, and the solid line corresponds to a method of extrapolation that interpolates the temperature and salinity profiles along the hypotenuse of the bottom triangle and infers the geostrophic shear.

4. Results and discussion

4.1. Regional circulation

The volume, heat- and salt-anomaly fluxes obtained after the inversion allow the study of the circulation across the western

sector of the SSR. The lateral fluxes along the box domain and the cumulative transports before and after the inversion are shown in Fig. 7, where we can observe that transits 1 and 3 introduce most of the initial imbalance. In order to determine the net flow through the sector of the Weddell–Scotia Confluence region covered by the box domain we have compared the net flow

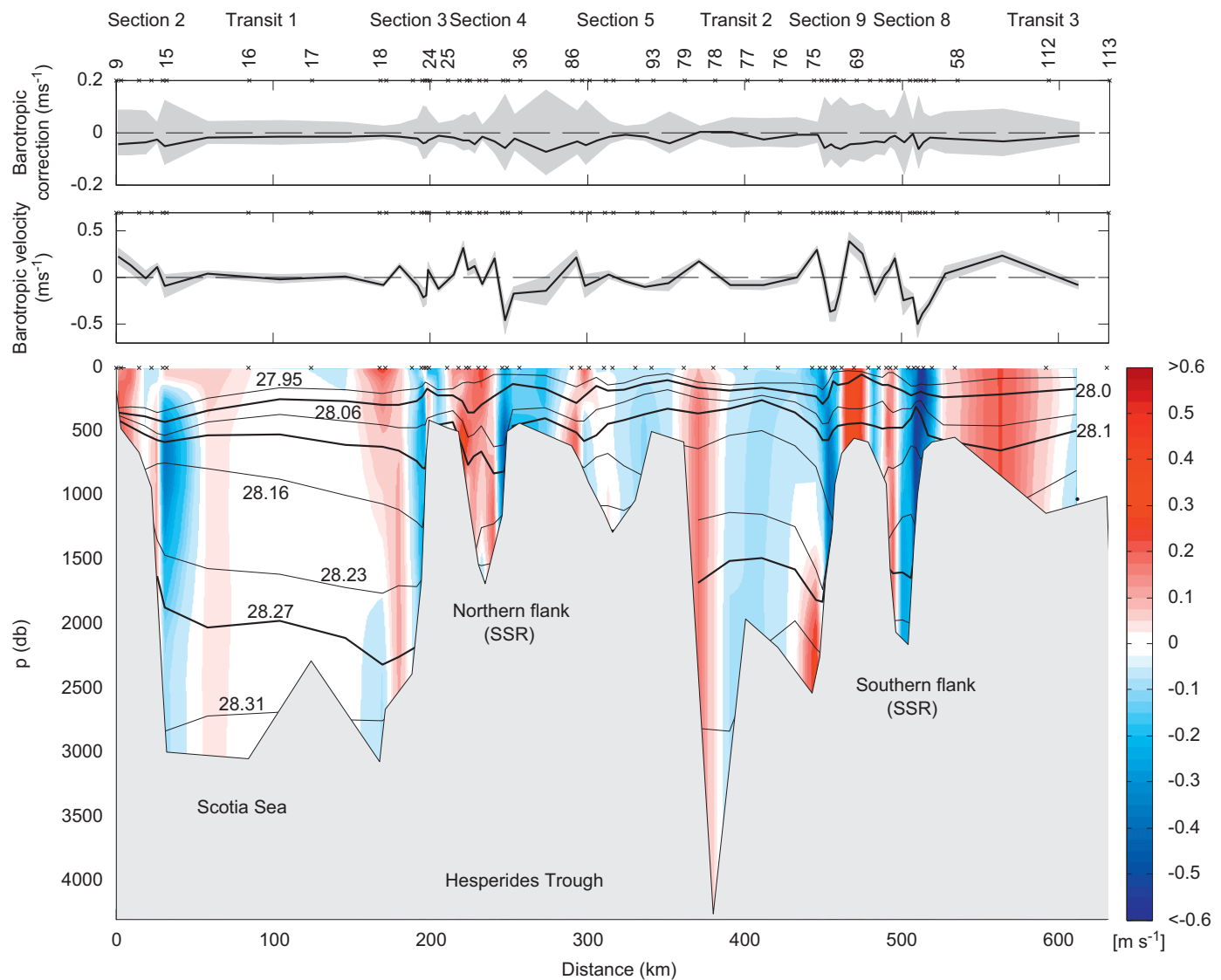


Fig. 6. The difference between the model solution with rank=5 and the first guess obtained from the ESASSI-08 data (top panel); the shaded areas denote the uncertainty of the first guess. The barotropic component obtained after the inversion of the model, with shaded areas denoting the uncertainty of the solution (middle panel). The barotropic component has been added to the geostrophic velocities computed from station pairs to yield the total geostrophic velocity field (lower panel); black lines are the neutral density model interfaces (the thicker ones correspond to 28.00, 28.10, and 28.27 kg m^{-3}). Positive values denote outward velocities from the box domain.

crossing its south-southeastern boundary with the net flow through the north-northeastern boundary (Fig. 8). In a scenario of perfect volume, heat, and salt conservation, the transports through these two boundaries should be the same. The selected rank of the solution does not reach that point, but the differences fall within the estimated a posteriori uncertainties (lower panels of Fig. 8) and are definitely much better than before the inversion (upper panels of Fig. 8).

The net fluxes through the region have been quantified as the mean value of the black and gray curves of Fig. 8, obtaining northward fluxes of 7 ± 5 Sv, 14 ± 5 TW, and $(0.8 \pm 0.4) \times 10^6 \text{ kg s}^{-1}$. The northward fluxes associated with the export of WDW have been quantified in 7 ± 4 Sv, 11 ± 6 TW and $(0.7 \pm 0.4) \times 10^6 \text{ kg s}^{-1}$, i.e., virtually the same as the full depth integrated transport. These positive heat- and salt-anomaly fluxes, most of them carried within layer 6 (lower panels of Fig. 8), do not mean that the Weddell Sea is injecting heat and salt into the Scotia Sea after leaving the Hesperides Trough. They are positive because the WDW entering the SSR from the Powell Basin is warmer and saltier than the mean temperature and salinity of the box domain, then resulting in positive potential

temperature and salinity anomalies, respectively. However, the WDW overflowing the SSR is cooler and fresher than the LCDW located further north (out of the box domain), then contributing to the cooling and freshening of the Scotia Sea. At intermediate levels, WDW and a part of LCDW ($28.1 < \gamma^{\text{n}} < 28.27 \text{ kg m}^{-3}$) occupy most of the lateral area of the box (Fig. 2). The volume transport across the different sections of the region is shown in the upper panel of Fig. 9.

Above the WDW, the subsurface layers (2, 3, and 4) indicate a net southward transport of AASW. In the southern flank of the ridge, the southward flow is mostly carried by the barotropic jet of transit 3 (casts 58–112), whereas in the northern flank there is an overall inflow into the ridge from the Scotia Sea. At surface (layer 1), however, the net volume transport is to the north. More important is the heat imbalance of 3.2 ± 1.6 TW, which indicates a heat gain of the surface water as it moves to the north, most likely from air–sea interactions.

Below the WDW, the WSDW enters into the ridge region from the Powell Basin (black line, lower panels of Fig. 8). In this case the flow across the north-northeastern boundary (gray line, lower panels of Fig. 8) only accounts for the net flow along the

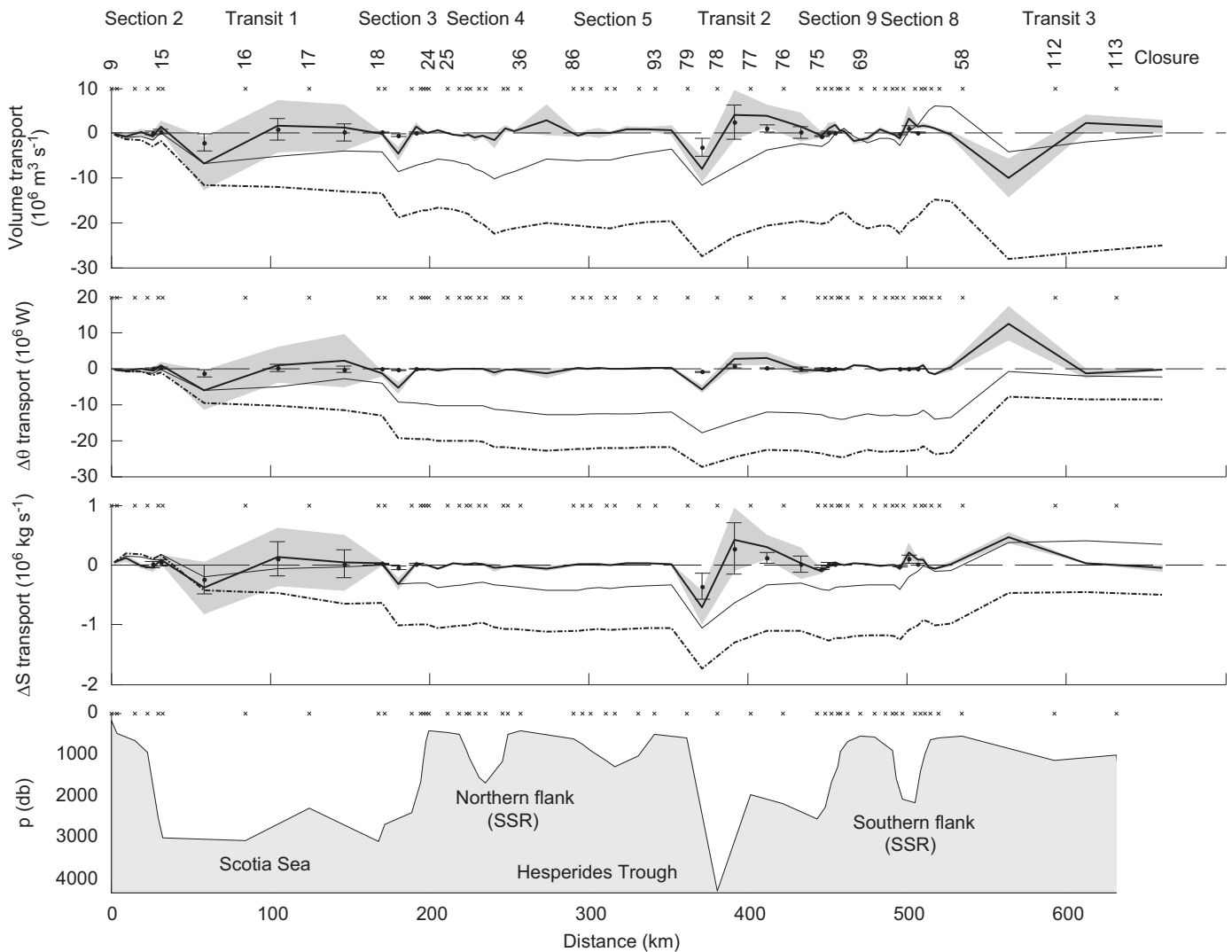


Fig. 7. Three upper panels: full depth water column flow along the box (thick solid line), its uncertainty (shaded area), and cumulative transports before (dash-dot line) and after (thin line) the inversion. Bars denote the transport (central point of the bar) and uncertainty associated with WSDW. The bathymetry is plotted in the lower panel.

Hesperides Trough, as WSDW is too deep to flow through the gaps of the northern boundary of the domain. The volume transport across the different sections of the region is shown in the lower panel of Fig. 9.

The water mass pathways are inferred from the joint analysis of the water mass distribution and the velocity field and fluxes obtained after the inversion. The analysis is complemented by the potential temperature and absolute velocity distributions across the ESASSI-08 section that crosses the Hesperides Gap, out of the box domain (Fig. 10) as well as by the previous knowledge of the circulation in the region (Gordon et al., 2001; Naveira Garabato et al., 2002a; von Gyldenfeldt et al., 2002).

In the WDW density range, there are two inflows from the Powell Basin into the Hesperides Trough (upper panel of Fig. 9): a net inflow of 3.8 ± 1.5 Sv through section 8 (51°W , 61.3°S), and a flow of 5 ± 2 Sv through 50°W (section 9 and the sector of transit 2 south of 60.6°S). Of these 5 Sv, 2.3 ± 1.3 Sv were measured flowing westwards between casts 77–76, in good agreement with the flow registered by a mooring deployed in this area (von Gyldenfeldt et al., 2002). An additional inflow (1.9 ± 1.4 Sv) enters into the ridge region through the shallow, southwestern sector of the box domain, likely coming from the Bransfield Strait and the tip of the Antarctic Peninsula. Most of that inflow (1.5 ± 1.0 Sv)

crosses the western sector of transit 3 (casts 113–112) and the rest flows between cast 113 and Elephant Island.

The most important outflow of WDW from the box domain is an eastward flow carrying 3.9 ± 0.6 Sv along the northern wall of the Hesperides Trough. From these, 1.5 ± 1.2 Sv recirculate clockwise within the trough (casts 78–77), while the rest spreads northwards into the Scotia Sea through the Hesperides Gap (Fig. 10). Secondary outflows over the northern flank of the box domain (sections 4 and 5) are also obtained, namely a deep outflow of 1.4 ± 1.0 Sv through section 4 and a fast (0.21 ± 0.08 m s⁻¹, Fig. 6) but narrow jet over the western shelf break of section 5. This narrow jet, negligible in terms of WDW transport (0.18 ± 0.13 Sv), was also recorded by drifters associated with a branch of the Antarctic Slope Current (Heywood et al., 2004; Thompson et al., 2009).

The source of formation for the lighter component of WSDW that reaches the northern side of the Powell Basin is the Larsen Ice Shelf, in the northwestern Weddell Sea, south of 64.5°S (Fahrbach et al., 1995). This recently formed WSDW has the buoyancy needed to cross the southern gaps of the SSR, west of the South Orkney Plateau (Naveira Garabato et al., 2002b). All these gaps are connected with the Hesperides Trough, which in turn is connected to the Scotia Sea only through the Hesperides Gap.

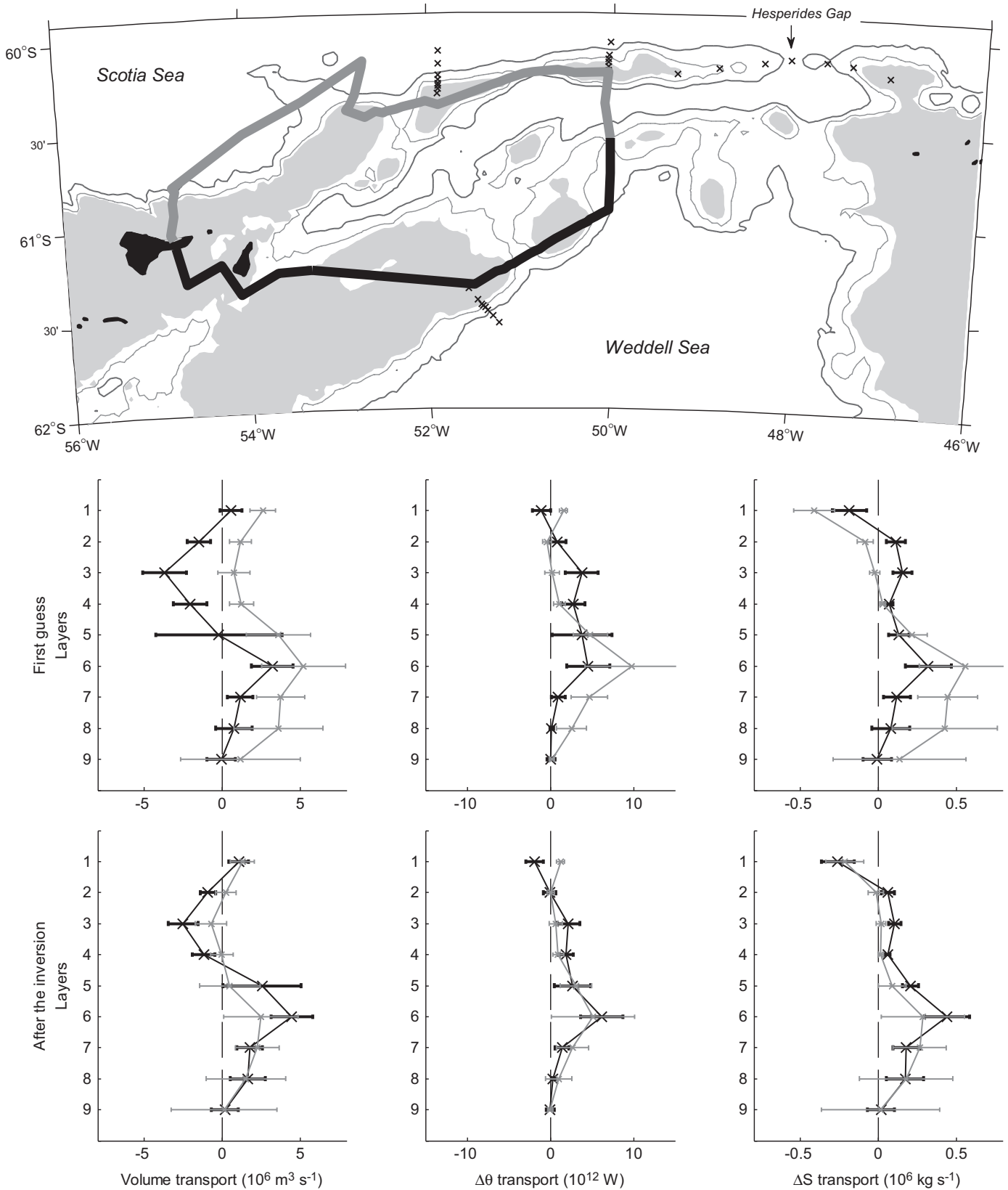


Fig. 8. Property transports across the southern (in black, positive entering the domain) and northern (in gray, positive exiting the domain) boundaries of the box before and after the inversion.

The colder and fresher WSDW component observed in the box injects $1.8 \pm 1.8 \text{ Sv}$ from the Powell Basin into the Hesperides Trough (lower panel of Fig. 9), $1.0 \pm 0.7 \text{ Sv}$ through section 8 (51°W) and $0.8 \pm 0.6 \text{ Sv}$ through transit 2 (50°W). Schodlok et al.

(2002) estimated the net transport of WSDW over the SSR west of the South Orkney Islands in 2.2 Sv , indicating that most of the inflow entering the ridge would be guided by the bathymetry of the trough. The $3 \pm 2 \text{ Sv}$ flowing eastwards along the northern

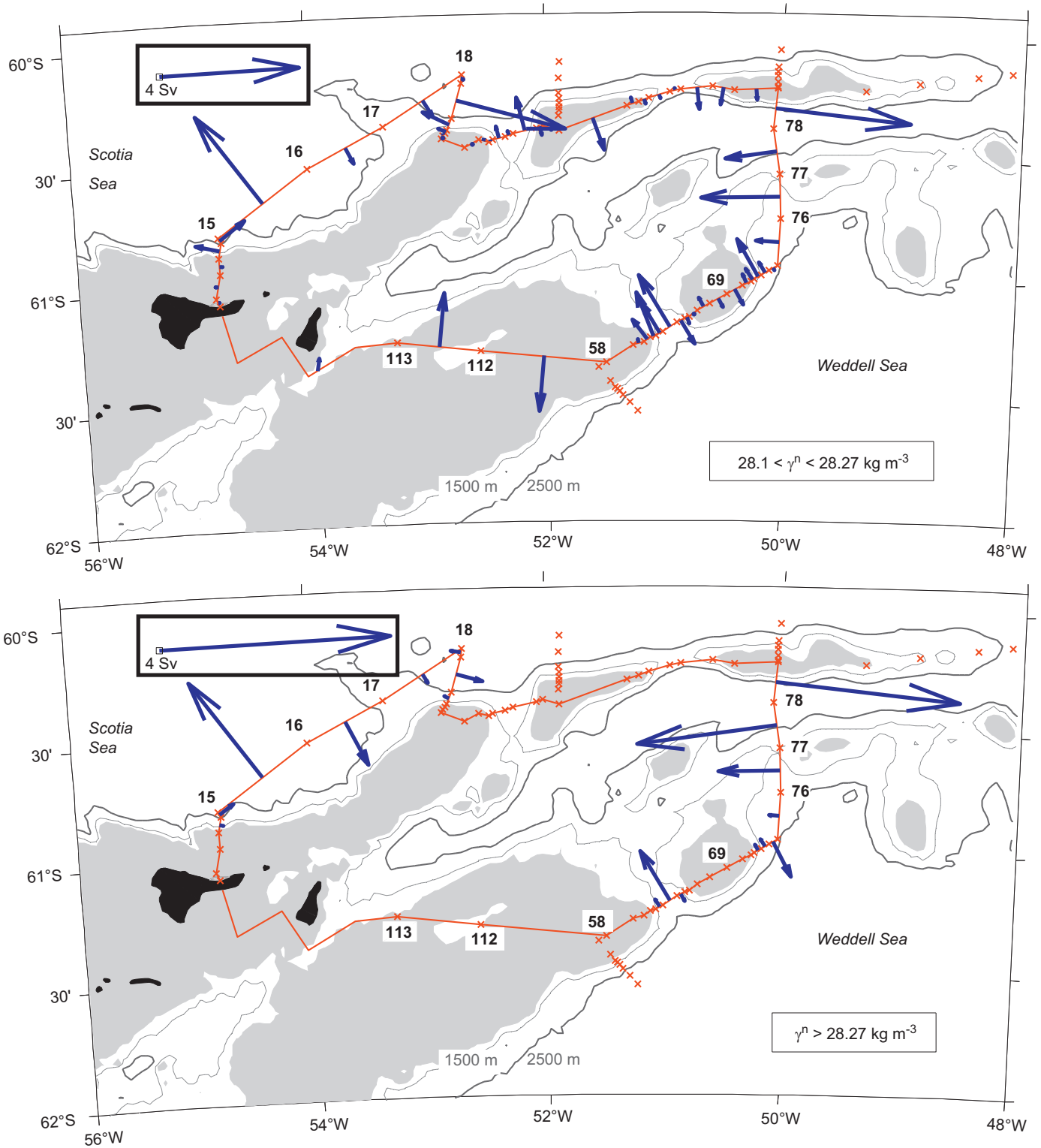


Fig. 9. Volume flows across the different passages of the domain for water masses with density greater than 28.10 kg m^{-3} . Upper panel: LCDW/WDW and modifications. Bottom panel: WSDW and modifications.

slope of the Hesperides Trough (casts 79–78) and the westward flow along the southern slope (casts 77–78, $2 \pm 4 \text{ Sv}$) indicate a significant amount of water recirculating around the trough.

The outward flow of WSDW from the box domain (transit 2, Fig. 9) and after that from the Hesperides Trough into the Scotia Sea through the Hesperides Gap (Fig. 10) is found below 1500 m, a shallower level than the upper level of the WSDW component

that outflows into the Scotia Sea through the Orkney Passage (Naveira Garabato et al., 2002b).

4.2. Water mass modification

The circulation inside the Hesperides Trough plays a key role in the exchange of hydrographic properties between the involved

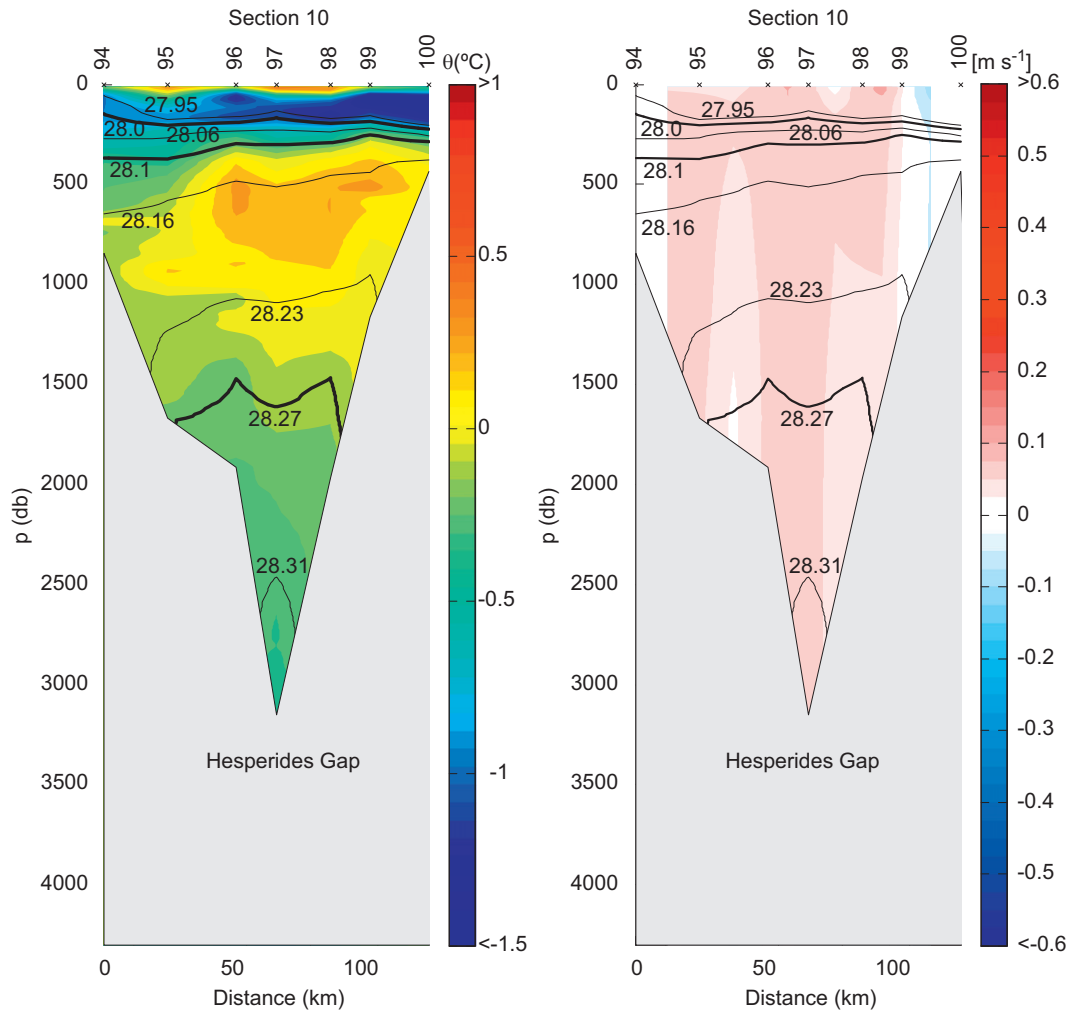


Fig. 10. ESASSI-08 section across the Hesperides Gap, located out of the box domain (see Fig. 1). Left panel: potential temperature distribution; right panel: the velocity field obtained following Rudnick's method (Rudnick, 1996; positive velocities are northward). Solid lines represent the neutral density model interfaces.

water masses. It has been shown that modified waters flowing northwards along the eastern continental slope of the Antarctic Peninsula inflow into the trough following the topography. Seaward, less modified water masses are injected into the trough from deeper areas of the Powell Basin. Both branches get close when crossing the southern gaps of the ridge and are forced to surround altogether the walls of the trough. This results in different mixtures exiting the box domain.

The inward and outward volume transports through the walls of the box domain plotted over a θ - S diagram are shown in Fig. 11. The first conclusion is that waters outflowing the domain are more homogenous (Fig. 11b) than on entrance (Fig. 11a), particularly for the temperature. The exception is around the 28.1 kg m^{-3} isopycnal, where the outflowing waters are colder and fresher (barotropic jet at the southeastward transit 3) or warmer and saltier (at the northern shelves) than on entrance. The diapycnal mixing component obtained after the inversion has a small impact on the property transports over the box area when compared with the lateral flows, then suggesting that the modification of the water masses takes place mostly along isopycnals.

The water masses delimited by the 28.16 and 28.23 kg m^{-3} isopycnals inflow into the ridge with temperatures ranging from about -0.3 °C to 0.5 °C (Fig. 11c), and outflow within a narrower range: from about -0.2 °C to 0.25 °C (Fig. 11d). The core of WDW lies within these isopycnals over the western sector of the SSR. Its potential temperature value is slightly below 0.5 °C when this

water mass inflows into the ridge through the southern flank (Fig. 11c, casts 62 and 76). The maximum is eroded inside the trough while mixing along isopycnals, cooling down to 0.25 °C (Fig. 11d, cast 78). The similarity of casts 78 (in the middle of the trough) and cast 77 supports the idea of some recirculation inside the trough (Fig. 11c and d).

Intense mixing processes associated with the presence of the Antarctic Slope Front (which flows over the western slope of section 8) would be responsible for the modification of the water masses before entering the SSR through that gap (Heywood et al., 2004). The WDW located offshore (0.4 °C, 34.67 , Fig. 11c, section 8, cast 62, 1400 m) is cooled and freshened, resulting in a modified water mass with potential temperature below 0 °C and salinity around 34.63 (Fig. 11e, section 8, cast 61, 980 m) that bifurcates into two branches. The same water mass is observed 120 km downstream following the 1000 m isobath inside the trough (Fig. 11e, transit 3, cast 113) and also filling the shallower areas of the western sector of the SSR (Fig. 11e, section 5, cast 91, 1300 m) as in Heywood et al. (2004). A secondary branch, maybe a bifurcation of this current, is also observed less than 20 km downstream following the 1500 m isobath over the eastern slope of section 8 (Fig. 11e, cast 65), outflowing to the southeast following the topography.

Once in the Scotia Sea, the colder and fresher WDW from the Hesperides Trough meets the warmer and saltier WDW component from the eastern gaps of the SSR (Naveira Garabato et al.,

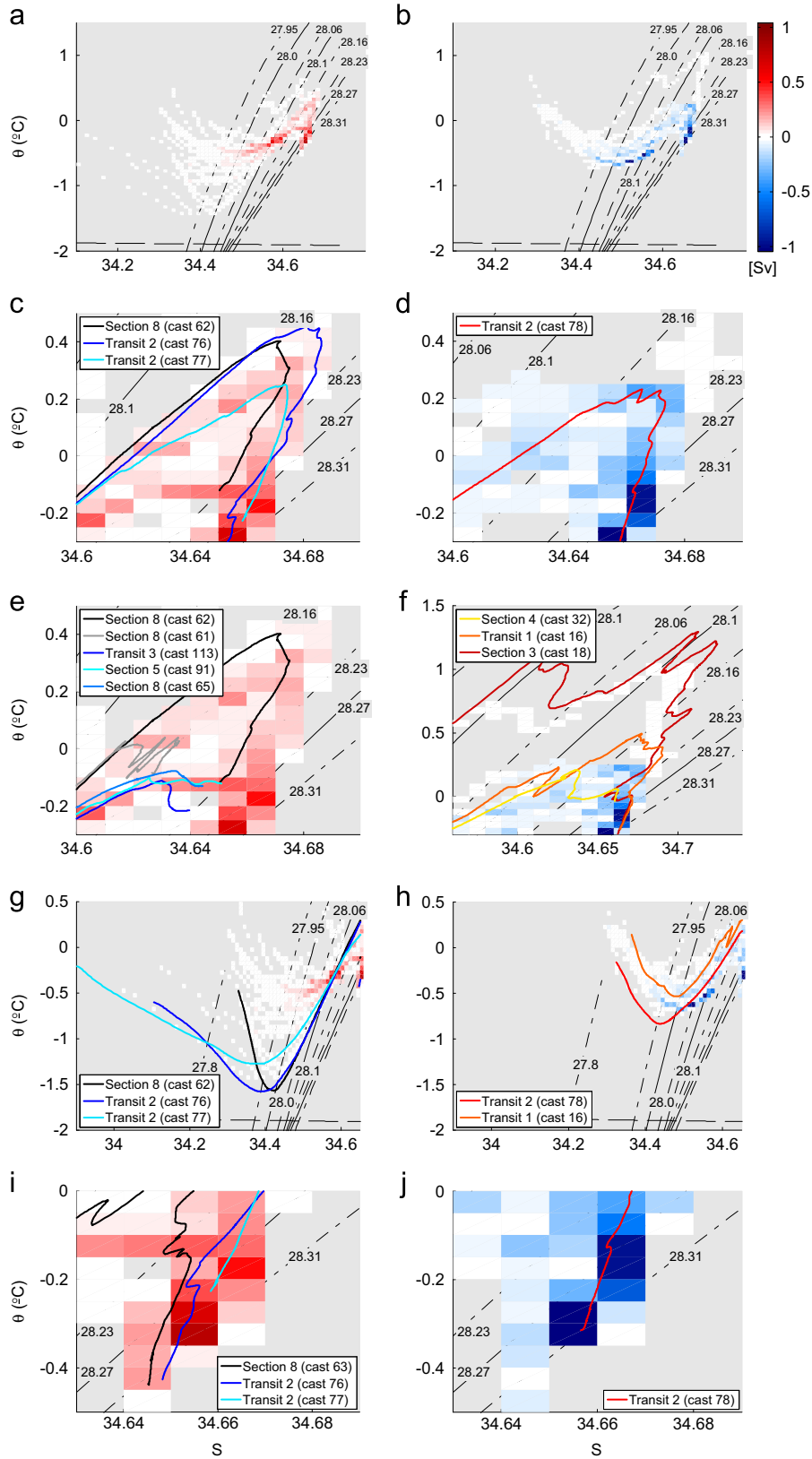


Fig. 11. Volume transport over a θ - S diagram: the diagram has been divided in $0.05^{\circ}\text{C} \times 0.01$ cells and each cell has been assigned the transport of water having the θ - S properties of the cell. The distribution of the exiting transport in a smaller/larger number of cells than on input indicates homogenization/dispersion of the water properties within the box domain. (a) Flow entering the box domain; (b) flow exiting the box domain; (c)–(j) zooms of panels (a) and (b), with different profiles of ESASSI-08 stations overlotted.

2003). The interaction between them and/or with CDW from the ACC further north results in different degrees of modification of the water masses. The deepest profile of section 4 (Fig. 11f, cast 32, 1600 m) presents two different cores of WDW: the lighter suggests mixing with WDW from the Orkney Passage, and the denser is a deeper branch of WDW from the Hesperides Trough. The proportion of the WDW component from the Orkney Passage is higher seaward (Fig. 11f, transit 1, cast 16, 3000 m). To the north of the box domain, the LCDW is modified by intrusions of WDW (Fig. 11f, cast 18, $\theta_{\max} > 1^\circ\text{C}$ and $S_{\max} > 34.7$, 3000 m).

Whereas in the western sector of the Weddell–Scotia Confluence the WDW cools and freshens before overflowing the northern flank of the ridge, the surface and subsurface waters become warmer and saltier (Patterson and Sievers, 1980). The comparison of the sea surface inflow with the more homogeneous surface outflow indicates mixing of water masses, but the heat gain from the atmosphere results in an outflow warmer than expected if only mixing processes were involved (Fig. 11h). On the other hand, the freshening of the first 50 m at stations 76 and 77 (Fig. 11g, transit 2, $\gamma^n < 27.8\text{ kg m}^{-3}$, $S < 34.2$) suggests the intrusion of melted water due to their proximity to the South Orkney Plateau, but this signature must quickly dilute as it is not observed anywhere else in the box.

The subsurface WW has a relative temperature minimum of -1.6°C when inflowing into the ridge through section 8 (Fig. 11g, cast 62, $S \approx 34.42$, depth $\approx 200\text{ m}$) and transit 2 (Fig. 11g, cast 76, $S \approx 34.39$, depth $\approx 100\text{ m}$). The value of that minimum warms to the north, where the summer mixed layer is slightly thicker and warmer than to the south (the sea-ice extended north of 62°S during the cruise, as inferred from the NCEP Reanalysis, NOAA/OAR/ESRL PSD, <http://www.esrl.noaa.gov/psd>). After surrounding the western side of the Hesperides Trough, this core warms ($\theta = -0.8^\circ\text{C}$) and becomes saltier ($S = 34.45$) (Fig. 11h, transit 2, cast 78). Once outside the trough, in the Scotia Sea, it reaches values of -0.5°C and 34.47 (Fig. 11h, transit 1, cast 16). Overall in the box domain, the relative cores of WW are more pronounced down slope and in seaward locations, whereas over the shelf break an homogenization in temperature ($\theta \approx -0.5^\circ\text{C}$) is observed and the salinities linearly increase with density at a rate of about $1\text{ (kg m}^{-3}\text{)}^{-1}$, ranging approximately from 34.4 to 34.6.

Below the WDW, the coldest and freshest component of WSDW observed in the box domain comes from the Powell Basin (Fig. 11i, section 8, cast 63, and transit 2, cast 76). The outflow from the Hesperides Trough is a water mass slightly warmer and saltier (Fig. 11j, transit 2, cast 78). Discarding isopycnal mixing processes on the basis that the inflowing bottom waters are colder and fresher than the northern profiles of the Hesperides Trough, diapycnal mixing is expected to be the responsible for the temperature and salinity changes suffered by the bottom waters while circulating in the trough. Some heat diffusion into the upper layer of WSDW from the lower layer of WDW is obtained after the inversion (Table 4, $0.02 \pm 0.05\text{ TW}$), and some salinity exchange at the deeper layers of the model (Table 4, $(0.007 \pm 0.007) \times 10^6\text{ kg s}^{-1}$).

5. Conclusions

The high spatial resolution of the ESASSI-08 data set has allowed the determination of the water mass pathways and property transports in the sector of the South Scotia Ridge west of 50°W . In order to obtain a better estimation, an inverse model has been applied to correct the barotropic velocities initially inferred from CTD and ADCP data.

Results show that intermediate and bottom Weddell Sea waters overflowing the SSR west of the South Orkney Islands

are forced to circulate clockwise around the Hesperides Trough, a process during which water masses undergo some property modifications. Subsurface WW and intermediate WDW (the latter accounts for most of the volume transport) exchange heat and salt mainly along isopycnals. As a consequence of the mixing, both the warmer and saltier WDW and the colder and fresher WW cores are eroded before outflowing into the Scotia Sea and the overall process results in a homogenization of the water masses crossing the ridge. The characteristics of the WDW when outflowing the SSR west of the South Orkney Islands suggest that they could contribute not only to the cooling and freshening of the ACC waters (Whitworth et al., 1994), but also to the modification of the Weddell Sea waters flowing across the Orkney Passage and turning west along the northern flank of the SSR, where they meet (Naveira Garabato et al., 2002a).

The bottom waters of the Weddell Sea (WSDW) and those in the Scotia Sea are not directly connected through the inverse model domain. It has been shown that when they enter the southern flank of the ridge and recirculate within the Hesperides Trough they incorporate some heat and salt from the lower layers of WDW, but on outflow they are still colder and fresher than the deep water of the Scotia Sea and hence they also contribute to the freshening and cooling of that basin.

When going to the details of the flow, the southern flank of the ridge presents two main entrance gates for WDW and WSDW: the 2100 m depth gap at 51°W , 61.2°S , where the Antarctic Slope Front is identified, and along the 50°W meridional section south of the Hesperides Trough. Most of these waters outflow to the Scotia Sea through the deepest gap (3000 m, out of the model domain but also sampled during the ESASSI-08 cruise) after circulating around the Hesperides Trough. In the northern flank of the ridge there are two additional shallower gaps playing different roles due to their topographical differences, but the volume transport of WDW is rather small through both gaps. The schemes of the inferred water mass circulation are shown in Fig. 12. The pathways of AASW are analogous to the water mass below and therefore not shown in a separate panel. WW is observed over-riding the WDW, both following the same pathways.

A net volume transport of $7 \pm 4\text{ Sv}$ of WDW has been obtained flowing from the Weddell Sea into the Scotia Sea across the box domain. When compared with the $10.5 \pm 5\text{ Sv}$ estimated by Naveira Garabato et al. (2003) for the whole South Scotia Ridge, it turns out that the western sector of the SSR plays a very significant role in the export of WDW to the Scotia Sea. The estimated heat- ('enthalpy') and salt-anomaly transports over the box are $11 \pm 6\text{ TW}$ and $(0.7 \pm 0.4) \times 10^6\text{ kg s}^{-1}$, with respect to the local mean values. The box domain is located beyond the southern boundary of the ACC, and therefore the obtained heat and salt transports must be understood in the context of the studied region. The mean values for the box domain are of $-0.29 \pm 0.16^\circ\text{C}$ and 34.56 ± 0.05 (Table 3), much colder but not significantly fresher than the $1.2 \pm 1.4^\circ\text{C}$ and 34.58 ± 0.14 given by Naveira Garabato et al. (2003) for the Scotia Sea. Hence, the waters overflowing this sector of the SSR are expected to contribute very significantly to the modification of the lower CDW layers through intense lateral mixing, a process observed by Orsi et al. (1999).

The comparison between the $1.8 \pm 1.8\text{ Sv}$ of WSDW entering the southern/southeastern boundaries of the model domain and the 2.2 Sv given by Schodlok et al. (2002) for a section running from the South Shetland to the South Orkney Islands, suggests that a large part of the bottom waters west of the South Orkney Plateau circulates clockwise around the Hesperides Trough, instead of reaching the ultimate gateway (the Hesperides Gap) through the Philip Passage. Note that the 2.2 Sv might be over-estimated according to the definition of WSDW used by Schodlok

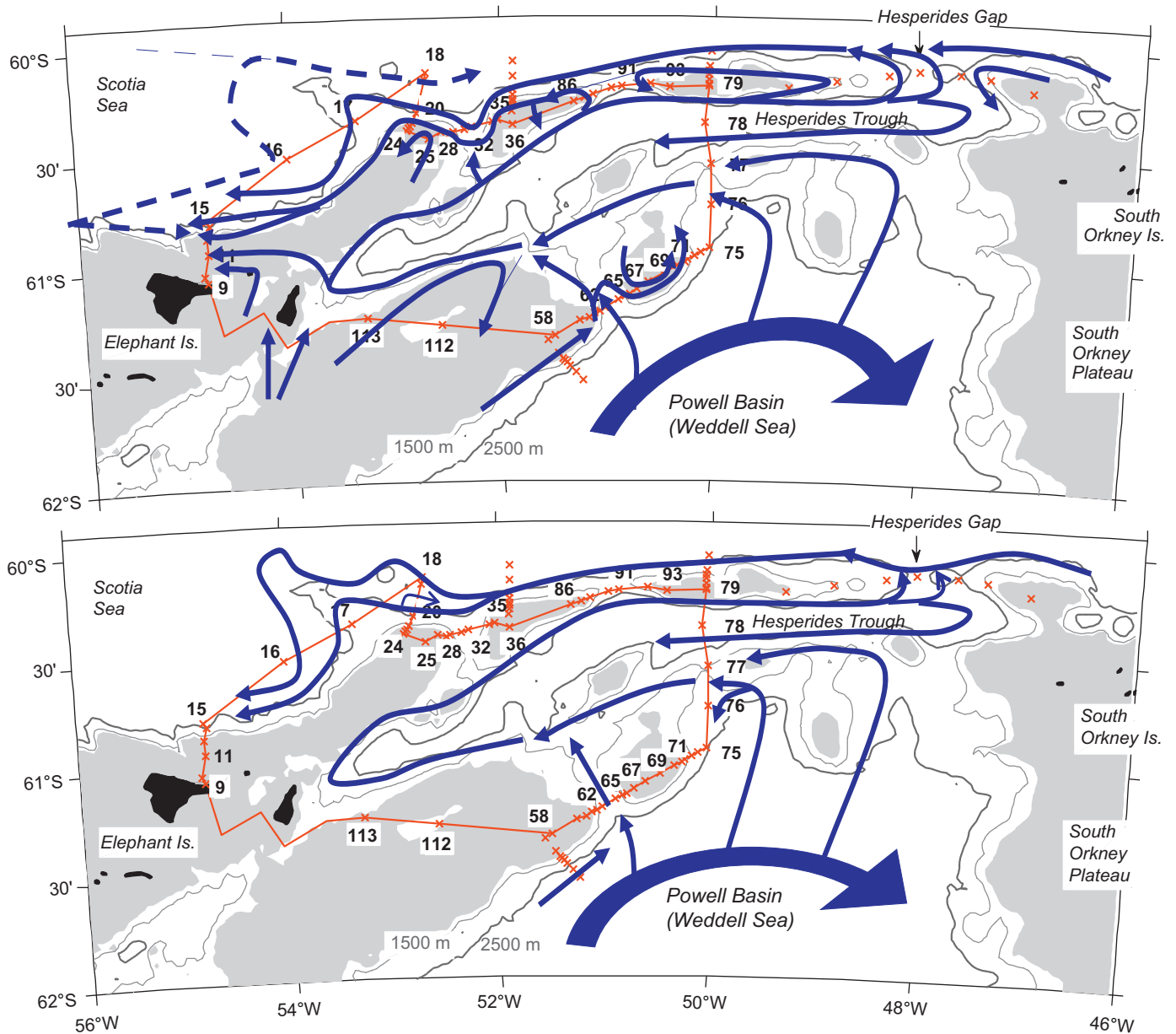


Fig. 12. Sketch of the water mass pathways inferred in this study. Upper panel: LCDW (blue dashed lines) and WDW (blue solid lines). Bottom panel: WSDW (blue solid lines). (For interpretation of the references to color in this figure legend, the reader is referred to the web version of this article.)

et al. (2002), based on potential temperature and salinity ranges instead of on neutral density. The obtained values also indicate that the amount of WSDW crossing the western sector of the SSR would be about a half of that flowing through the Orkney Passage (3.48 Sv according to Franco et al. (2007) and 5.6 Sv according to Naveira Garabato et al. (2002b)). When making both statements, however, one must take into account the uncertainties associated with the estimated values.

The modification of the water masses inside the Hesperides Trough inferred from the θ - S analysis is supported by the observations along the 48°W section obtained by the US DOVETAIL cruise (1997). The clear discontinuity in the vertical distribution of the water mass properties when this section crosses the Hesperides Trough from the Philip Passage to the Hesperides Gap discards a straight, northward flow across the trough. The vertical distribution of LADCP zonal velocities is of special interest: it shows a clear eastward flow along the northern slope of the trough, with

velocities higher than 0.10 m s^{-1} for most of the water column and a more localized westward current along the southern slope of the trough, then supporting our results.

Acknowledgments

This work has been carried out in the framework of the ESASSI project (POL2006-11139-C02-01/CGL, CGL2007-28783-E/ANT, CTM2008-04623-E/ANT, and CTM2009-08287-E/ANT) funded by the Spanish Polar Research Program and by the FEDER program of the European Union. We thank the scientists, technicians, officers and crew of R/V *Hesperides* for their help and expertise during the ESASSI-08 cruise. We specially thank Dr. Andrew F. Thompson for providing the historical and ADELIE drifter datasets, and Drs. Martin Visbeck and Bruce Huber for providing the DOVETAIL LADCP data. M. Palmer acknowledges an FPI grant funded by the Spanish

Ministry of Science and Innovation. M.M. Flexas acknowledges a postdoctoral contract funded by the Government of the Balearic Islands and a José Castillejo grant at the Jet Propulsion Laboratory (NASA) funded by the Spanish Ministry of Science and Innovation. G. Jordà acknowledges a JAE-Doc contract funded by the Spanish Research Council. We are very grateful to the three anonymous reviewers for their useful comments and suggestions, which have helped to improve the quality of this paper.

References

- Deacon, G.E.R., Foster, T.D., 1977. The boundary region between the Weddell Sea and Drake Passage currents. *Deep-Sea Res.* 24, 505–510.
- DOVETAIL, 1997. Deep Ocean Ventilation Through Antarctic Intermediate Layers. U.S. Cruise Report, available from: <<http://www.ideo.columbia.edu/res/fac/physocean/Dovetail/cruiserep.htm>>.
- Fahrbach, E., Rohardt, G., Scheele, N., Schröder, M., Strass, V., Wisotzki, A., 1995. Formation and discharge of deep and bottom water in the northwestern Weddell Sea. *J. Mar. Res.* 53, 515–538.
- Franco, B.C., Mata, M.M., Piola, A.R., Garcia, C.A.E., 2007. Northwestern Weddell Sea deep outflow into the Scotia Sea during the austral summers of 2000 and 2001 estimated by inverse methods. *Deep-Sea Res.* 55, 1815–1840.
- Ganachaud, A., Wunsch, C., 2000. Improved estimates of global ocean circulation, heat transport and mixing from hydrographic data. *Nature* 408, 453–457.
- Golub, G.H., Kahan, W., 1965. Calculating the singular values and pseudo-inverse of a matrix. *J. Soc. Ind. Appl. Math. Ser. B Numer. Anal.* 2 (2), 205–224.
- Gordon, A.L., Visbeck, M., Huber, B., 2001. Export of Weddell Sea deep and bottom water. *J. Geophys. Res.* 106, 9005–9018.
- Heywood, K.J., Naveira Garabato, A.C., Stevens, D.P., Muench, R.D., 2004. On the fate of the Antarctic Slope Front and the origin of the Weddell Front. *J. Geophys. Res.* 109, C06021.
- Jullion, L., Heywood, K.J., Naveira Garabato, A.C., Stevens, D.P., 2010. Circulation and water mass modification in the Brazil–Malvinas Confluence. *J. Phys. Oceanogr.* 40, 845–864.
- Lawson, C.L., Hanson, R.J., 1974. *Solving Least Squares Problems*. Prentice-Hall, Englewood Cliffs, NJ.
- Locarnini, R.A., Whitworth III, T., Nowlin Jr., W.D., 1993. The importance of the Scotia Sea on the outflow of Weddell Sea Deep Water. *J. Mar. Res.* 51, 135–153.
- López, O., García, M.A., Gomis, D., Rojas, P., Sospedra, J., Arcilla, A.S., 1999. Hydrographic and hydrodynamic characteristics of the eastern basin of the Bransfield Strait (Antarctica). *Deep-Sea Res.* 46, 1755–1778.
- McDougall, T.J., 1987. Neutral surfaces. *J. Phys. Oceanogr.* 17, 1950–1964.
- McDougall, T.J., 1991. Parameterizing mixing in inverse models. Dynamics of oceanic internal gravity. In: Waves, P., Muller, Henderson, D. (Eds.), 'Aha Huliko'a Winter Workshop, University of Hawaii, pp. 355–386.
- McIntosh, P.C., Rintoul, S.R., 1997. Do box inverse models work? *J. Phys. Oceanogr.* 27, 291–308.
- Morgan, P.P., 1994. Box Inverse Modeling with DOBOX 4.2. CSIRO Marine Laboratories Report 225, 26.
- Mosby, H., 1934. The waters of the Atlantic Antarctic Ocean. *Sci. Res. Norw. Antarct. Exped 1927–1928 (1934)*, 1–131.
- Muench, R.D., Hellmer, H.H., 2002. The international DOVETAIL program. *Deep-Sea Res.* 49 (21), 4711–4714.
- Naveira Garabato, A.C., Heywood, K.J., Stevens, D.P., 2002a. Modification and pathways of Southern Ocean deep waters in the Scotia Sea. *Deep-Sea Res.* 49 (4), 681–705.
- Naveira Garabato, A.C., McDonagh, E.L., Stevens, D.P., Heywood, K.J., Sanders, R.J., 2002b. On the export of Antarctic Bottom Water from the Weddell Sea. *Deep-Sea Res.* 49 (21), 4715–4742.
- Naveira Garabato, A.C., Stevens, D.P., Heywood, K.J., 2003. Water mass conversion, fluxes, and mixing in the Scotia Sea diagnosed by an inverse model. *J. Phys. Oceanogr.* 33, 2565–2587.
- Orsi, A.H., Nowlin Jr., W.D., Whitworth III, T., 1993. On the circulation and stratification of the Weddell Gyre. *Deep-Sea Res.* 40 (1), 169–203.
- Orsi, A.H., Whitworth III, T., Nowlin Jr., W.D., 1995. On the meridional extent and fronts of the Antarctic Circumpolar Current. *Deep-Sea Res.* 42, 641–673.
- Orsi, A.H., Johnson, G.C., Bullister, J.L., 1999. Circulation, mixing, and production of Antarctic Bottom Water. *Prog. Oceanogr.* 43, 55–109, Pergamon.
- Padman, L., Fricker, H.A., Coleman, R., Howard, S., Erofeeva, S., 2002. A new tidal model for the Antarctic ice shelves and seas. *Ann. Glaciol.* 34, 247–254.
- Patterson, S.L., Sievers, H.A., 1980. The Weddell–Scotia Confluence. *J. Phys. Oceanogr.* 10, 1584–1610.
- Reid, J.L., Nowlin Jr., W.D., Patzert, W.C., 1977. On the characteristics and circulation of the southwestern Atlantic Ocean. *J. Phys. Oceanogr.* 7, 62–91.
- Rudnick, D.L., 1996. Intensive surveys of the Azores front, 2. Inferring the geostrophic and vertical velocity fields. *J. Geophys. Res.* 101 (C7), 16,291–16,303.
- Savidge, D.K., Amft, J.A., 2009. Circulation on the west Antarctic Peninsula derived from 6 years of shipboard ADCP transects. *Deep-Sea Res.* 56, 1633–1655.
- Schodlok, M.P., Hellmer, H.H., Beckmann, A., 2002. On the transport, variability and origin of dense water masses crossing the South Scotia Ridge. *Deep-Sea Res.* 49B, 4807–4825.
- Sloyan, B.M., Rintoul, S.R., 2000. Estimates of area-averaged diapycnal fluxes from basin-scale budgets. *J. Phys. Oceanogr.* 30, 2320–2341.
- Smith, W.H.F., Sandwell, D.T., 1997. Global sea floor topography from satellite altimetry and ship depth soundings. *Science* 277, 1956–1962.
- Thompson, A.F., Heywood, K.J., 2008. Frontal structure and transport in the northwestern Weddell Sea. *Deep-Sea Res.* 55, 1229–1251.
- Thompson, A.F., Heywood, K.J., Thorpe, S.E., Renner, A.H.H., Trasviña, A., 2009. Surface circulation at the tip of the Antarctic Peninsula from drifters. *J. Phys. Oceanogr.* 39, 3–26.
- von Gyldenfeldt, A.-B., Fahrbach, E., García, M.A., Schröder, M., 2002. Flow variability at the tip of the Antarctic Peninsula. *Deep-Sea Res.* 49, 4743–4766.
- Whitworth III, T., Nowlin, W.D., Orsi, A.H., Locarnini, R.A., Smith, S.G., 1994. Weddell Sea Shelf Water in the Bransfield Strait and Weddell–Scotia Confluence. *Deep-Sea Res.* 41, 629–641.
- Whitworth III, T., Orsi, A.H., Kim, S.J., Nowlin Jr., W.D., Locarnini, R.A., 1998. Water masses and mixing near the Antarctica Slope Front. In: Jacobs, S.S., Weiss, R.F. (Eds.), *Interactions at the Antarctic Continental Margins*, vol. 74. Antarctic Research Series. American Geophysical Union, pp. 1–27.
- Wunsch, C., 1977. Determining the general circulation of the oceans: a preliminary discussion. *Science* 196, 871–875.
- Wunsch, C., 1996. *The Ocean Circulation Inverse Problem*. Cambridge University Press, Cambridge 437 pp.